



# The influence of wind speed on the power of wind turbines installed on sloped-roof buildings

Minh Ky Nguyen<sup>1</sup>, Thanh Danh Le<sup>2</sup>, and De Tai Duong<sup>3\*</sup>

<sup>1</sup> Ho Chi Minh City University of Technology and Education, Viet Nam

<sup>2</sup> University of Economics Ho Chi Minh City, Viet Nam

<sup>3</sup>Tran Dai Nghia University, Viet Nam

\*duongdetai@tdnu.edu.vn

**Abstract.** Understanding wind effects on buildings is crucial for mitigating wind-induced damage. This study focuses on the aerodynamic impact of wind on low-rise buildings, with a particular emphasis on vulnerable roof sheathing. Using a  $k-\epsilon$  turbulence model, the pressure distribution on a  $27^\circ$  sloped roof is investigated at different free-stream flow velocities. The  $27^\circ$  sloped roof was selected as it represents the average roof pitch commonly found in Southeast Asia, especially in Vietnam. Results are compared using coarse and fine grid configurations around the building. Additionally, Horizontal Axis Wind Turbine (HAWT) with a 1.5m blade diameter is installed 3m above the roof, and its power coefficient is calculated using the actuator disk concept. Comparisons are made between undisturbed flow and flow above the sloped roof. The research findings emphasize the substantial impact of wind speed on the pressure distribution along the sloped roof and the power coefficient of the Horizontal Axis Wind Turbine (HAWT) along the roof surface. This study contributes to a better comprehension of the effects of wind speed on low-rise buildings and provides valuable insights for optimizing HAWT design, especially in the context of sloped roofs..

**Keywords:** Actuator Disk, Power Coefficient, Pressure Coefficient, Pitched-roof, Wind Turbine.

## 1 INTRODUCTION

The airflow is naturally generated and surrounds buildings (external flow). In some places worldwide, wind turbines are also installed on buildings to harness wind energy. In this case, wind speed is crucial as each wind turbine requires an appropriate and specific wind speed to rotate.

Today, the rising demand for energy consumption emphasizes the importance of optimizing various energy sources, given the development of science and technology and the depletion of non-renewable natural resources. Traditional power and thermal

power plants cannot meet current demands and have detrimental environmental effects. Therefore, the trend of using renewable energy sources such as wind and solar power is being extensively researched and implemented. Wind energy is known as one of the clean green energy forms as it does not emit greenhouse gases and does not rely on fossil fuels. Most houses using wind energy from wind turbines are still connected to the power grid when wind energy is insufficient. Recently, with technological advancements, manufacturing, and installation of wind turbines in residential areas, on the ground, or on rooftops have become more accessible and familiar. The power output of a building-mounted wind turbine is affected by the turbine's position, as the wind velocity profile at these positions varies. However, the aerodynamic performance of small wind turbines above buildings still needs to be better understood due to the complex flow field surrounding the building and the turbulent models affecting the wind turbine [1-7].

This study focuses on investigating the aerodynamic impact of a  $27^\circ$  sloped roof-building model on the power output of a wind turbine at various wind speeds. The primary objective is to analyze the distribution of variable surface pressure on the roof to gain insights into how the sloped roof influences the turbine's performance. The  $27^\circ$  sloped roof was opted for due to its resemblance to the prevalent roof pitch found in Southeast Asia, with a particular focus on Vietnam. Understanding the aerodynamic behavior of the building-turbine system can lead to more efficient utilization of wind energy and contribute to mitigating wind-induced damage on the building envelope. The findings will provide valuable information for advancing sustainable wind energy solutions and optimizing renewable energy sources in the context of increasing global energy demands.

## 2 TURBULENCE MODEL AND ASSUMPTIONS

In some windward areas, the wind blowing around the building is relatively weak, not enough to turn the wind turbine. The wind speed is less than the limit speed of conventional wind turbines, so the turbine will not start to operate efficiently. There is a concept in wind engineering called the Hill effect [14]. It describes that the wind speed is lower than at the top in the area around the hill. Because of this, the winds compress on the side where the wind is blowing on the hill, and it can again expand into the low-pressure area of the leeward side of the hill. The same can be said for a building with an inclination angle so that there is suction pressure on the top of the building, giving a more incredible velocity in that place. However, if the wind turbine is placed on top of the building, it faces some turbulent flow due to the wind hitting the building. In this study, we have some constant and variable parameters. The simulations were performed under the following assumptions:

- + The position of the turbine along the roof is fixed in all cases. It is 3 m high from the top of the building.

- + The turbine side axis is assumed to be misaligned.

- + The angle of inclination of the building in all cases is  $27^\circ$ .

The turbine disc diameter of the actuator is 1.5 m in all cases.

- + The size of the entire building is constant in all different simulations.
- + The building is considered isolated so that there is no additional turbulent flow due to impacts from other buildings.
- + The wind's inlet velocity (free flow) to the calculated domain was assumed to be replaced by the variable velocities of 4, 5, 6, 7, 8, 9, 10, 11, and 12 m/s.
- + The k- $\epsilon$  turbulent flow model is used for investigation because it gives reliable results when considering the effect of roof elevation on the turbulent kinetic energy of the flow field when the separation phenomenon occurs from the front edge of the building and the separate vortices along the back of the building due to reverse flow. The k- $\epsilon$  entanglement model is a semi-empirical model with two transport equations to represent the properties of the turbulent flow. The transport variables k (representing perturbation energy) and  $\epsilon$  (representing perturbation scale) are the perturbation kinetic energy and perturbation dissipation, respectively. The influence of molecular viscosity is not considered when generating the k- $\epsilon$  model, so the standard k- $\epsilon$  model is valid for thoroughly turbulent flows. This model is helpful for flows in a free-sliding layer with relatively small pressure gradients.

From the following equations, k, and  $\epsilon$  are deduced [8-10]:

$$\frac{\partial}{\partial t}(\rho k) + \frac{\partial}{\partial x_i}(\rho k u_i) = \frac{\partial}{\partial x_j} \left[ \left( \mu + \frac{\mu_t}{\sigma_k} \right) \frac{\partial k}{\partial x_j} \right] + G_k + G_b - \rho \epsilon - Y_M + S_k \quad (1)$$

$$\frac{\partial}{\partial t}(\rho \epsilon) + \frac{\partial}{\partial x_i}(\rho \epsilon u_i) = \frac{\partial}{\partial x_j} \left[ \left( \mu + \frac{\mu_t}{\sigma_\epsilon} \right) \frac{\partial \epsilon}{\partial x_j} \right] + C_{1\epsilon} \frac{\epsilon}{k} (G_k + C_{3\epsilon} G_b) - C_{2\epsilon} \rho \frac{\epsilon^2}{k} + S_\epsilon \quad (2)$$

where  $u_i$  is the average velocity vector with components in the X and Y directions and  $G_k$  generation turbulence kinetic energy due to the average velocity gradient,  $G_b$  is generation turbulence energy due to buoyancy force.  $Y_M$  is contribution of the oscillating expansion in the compression perturbation to the overall dissipation rate.  $C_{1\epsilon}$ ,  $C_{2\epsilon}$  and  $C_{3\epsilon}$  are constants.  $\sigma_k$  and  $\sigma_\epsilon$  are turbulent Prandtl numbers for k and  $\epsilon$ .  $S_k$  and  $S_\epsilon$  user-defined source terms. In addition, the viscosity of turbulent (vortex) flow is calculated by:

$$\mu_t = \rho C_\mu \frac{k^2}{\epsilon} \quad (3)$$

where  $C_\mu$  is a constant, the value of the model default constant is defined as follows:  $C_{1\epsilon}=1.44$ ,  $C_{2\epsilon}=1.92$ ,  $C_\mu = 0.09$ ,  $\sigma_k = 1$ ,  $\sigma_\epsilon = 1.3$

### 3 MODEL OF INCLINED ROOF BUILDING WITHOUT HAWT

The building plan with a  $27^\circ$  roof inclination has been shown in Figure 1 with raw mesh. The dimensions of the building and the calculated domain are approximated according to the building in reference [4]. The building has a width of 7 m, and other specifications for the building dimensions and the calculation domain are shown in Figure.1. In addition, Figure 1 shows the grid surrounding the building, which is used for the computational domain. The number of grid cells is 50500.

The standard k- $\epsilon$  turbulence model with standard wall functions was used to predict the turbulent flow and separation zones around the building. Since the objective of

this study was to compare the power factor of wind turbines in the free flow and above the building, a standard k- $\epsilon$  disturbance model was chosen.

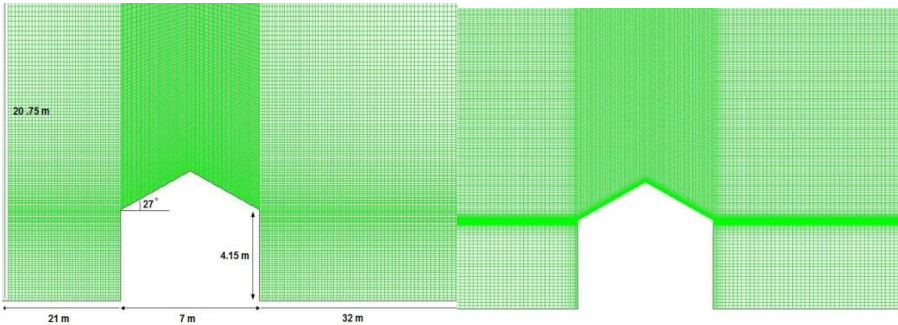


Fig.1. Building model and rough mesh around the building

Fig.2. Building model and fine mesh surrounding the building

The building model with the mesh near the walls is shown in Figure.2. The number of nodes and grid cells is 83151 and 82500, respectively. The wall-to-wall refined grid has a first cell height of  $1 \times 10^{-4}$  and a wall-to-wall ratio 1.15.

The reason for using the same model with refined mesh near the building wall is to compare the influence of the mesh on the pressure coefficient along the roof. The exact initial mesh has been used in this work and reference [4]. Its results and the results of building with refined mesh can compare. It expects that the refined mesh around the building shows more separated flows and recirculation regions around the building, which will influence the wind turbine's power coefficient when mounted on the building.

In Figure 3, the pressure coefficient ( $C_p$ ) distribution on the roof of the building is shown for the coarse mesh, as the free wind enters the calculation domain at different wind speeds ranging from 4 m/s to 12 m/s. The  $C_p$  coefficient experiences a significant drop from the front edge of the roof to the top of the roof. This drop is attributed to the angle of inclination of the roof, resulting in the highest suction pressure on the top of the building, which is the intended location for the turbine disc. Moving downstream on the roof, the pressure gradually increases. This behavior is due to the difference in cross-sectional area of the airflow upstream and downstream of the roof's rear edge.

Figure 4 illustrates the pressure coefficient distribution on the roof of the building as the free wind enters the calculation domain at various wind velocities, ranging from 4 m/s to 12 m/s, with a refined mesh near the walls of the building. The pressure on the front edge of the roof exhibits a sharp increase, covering approximately two-thirds of the roof's front edge, followed by a slight decrease towards the rooftop, and eventually transitioning into a suction effect on the rooftop. The leading edge of the roof maintains a nearly constant pressure, with only minor fluctuations observed at the roof's end for some high wind velocities, such as 11 m/s and 12 m/s.

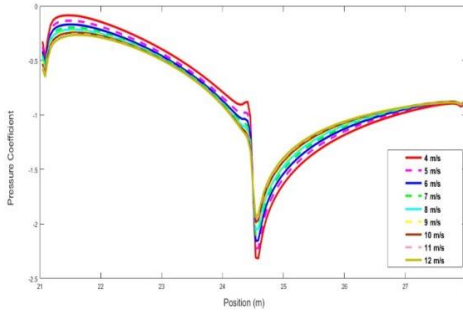


Fig.3. Pressure coefficient  $C_p$  for the case of the coarse mesh surrounding the building as Figure 1

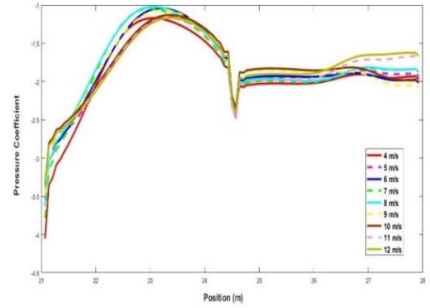


Fig.4. The pressure coefficient  $C_p$  for the case of the mesh surrounding the building as Figure 2

From the comparison of the results obtained for nets and screens near the wall, it is possible to determine the influence of the mesh on the distribution of pressure coefficients along the roof-court structure. The predicted pressure on the roof depends on the mesh size on the wall. Increasing the number of nodes in the wall produces almost no appreciable change in the pressure coefficient. The  $k-\epsilon$  perturbation model requires a fine mesh near the wall to give a better prediction. This model effectively predicts segregated flows above the building. Figure 5 shows the flow around the building, the separation zone, and the backflow at the rear edge of the roof.

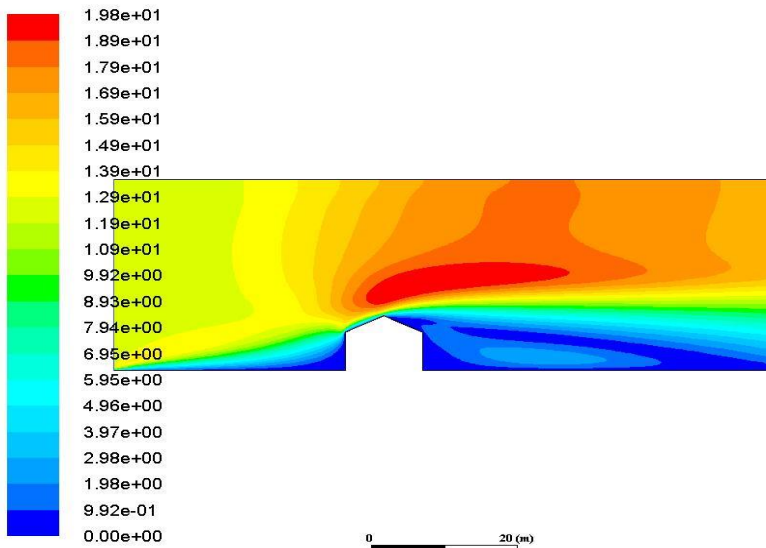


Fig.5. Flow velocity field around the building

## 4 MODEL OF INCLINED ROOF BUILDING WITH WIND TURBINES

Figure 6 shows the grid around the building of the same size as in Subsection 3.1. A drive disc with a radius of 0.75m is used, instead of a complete wind turbine model, to model the turbine load on the flow. The position and size of the actuator disk are considered constant for the simulations of all the different input velocities for the computational domain. The total number of nodes and cells applied to construct the mesh around the building and the actuator disk is 89469 and 88800, respectively. The first cell height around the building is  $1 \times 10^{-4}$ , and the grid ratio near the wall is 1,15.

A standard  $k-\epsilon$  turbulence model with a standard wall function will be used to predict the flow through the actuator disc and the flow surrounding the building. This model will have an essential effect on turbine performance. In addition, for the actuator disk model [11] to include the wall, the boundary condition of the fan is used. The method uses the wind turbine's power factor value to calculate the pressure difference between the inlet and outlet of the drive disc.

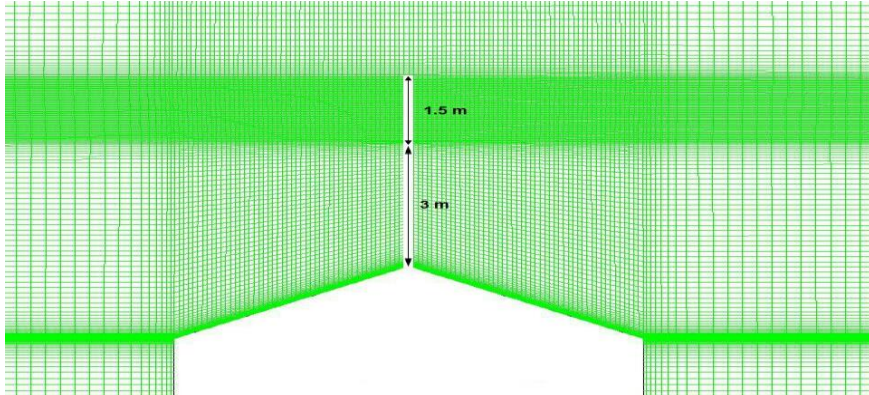


Fig.6. Mesh around the building with turbines.

Figure 5 shows that the average wind velocity intensity at the top of the roof, where the turbine is located, is significantly larger than the free flow velocity intensity. Figure 7 shows the velocity distribution field when the drive disc is mounted above the building. Results Figure 7 a, b, c, d with different free flow velocities of 4, 6, 8 and 9 m/s entering the domain. The flow velocity above the roof is significantly higher than without the wind turbine.

Velocity along the drive disc is uniform but decreases significantly when it interacts with the flow being separated from the building. The segregated zone behind the building is heavily influenced by turbine flow. In contrast, the flow characteristics above the building, especially at the front edge of the roof, are minimally influenced by turbine flow.

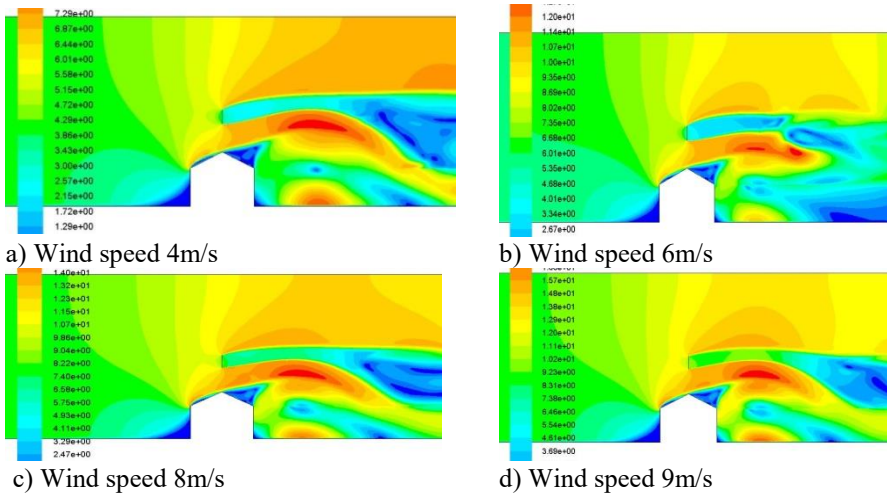


Fig.7. The flow velocity field surrounds the building and the wind turbine in the input velocity fields 4,6, 8 and 9 m/s, respectively.

Figures 8 and 9 show the pressure coefficient results along the roof of a building with a drive disc compared with the pressure coefficient without a drive disc. Figure 9 shows that the pressure along the roof increased approximately at each point when an actuator disc was installed. This increase is significant at 4 and 5 m/s, but the pressure difference with and without the drive disc is slight at higher speeds.

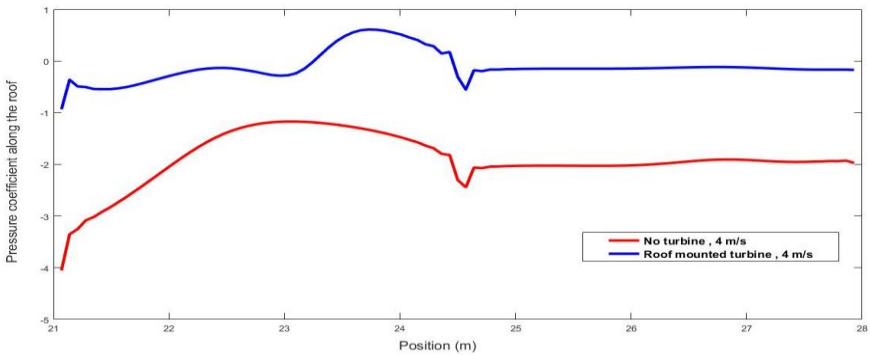


Fig.8. Pressure coefficient in the case of turbines and without wind turbines when the inlet wind speed is 4 m/s

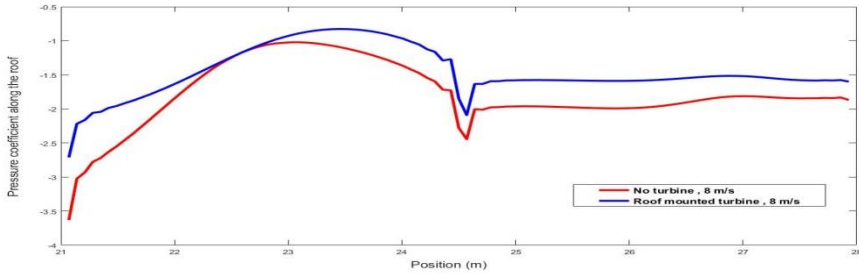


Fig.9. Pressure coefficient in the case of turbines and without wind turbines when the inlet wind speed is 9 m/s

From the obtained results, we can calculate the capacity of the wind turbine based on the following conversion formula [8-9]:

$$P = \frac{1}{2} \rho A V^3 C_p \quad (4)$$

Where  $P$ ,  $V$ ,  $\rho$ ,  $A$ , and  $C_p$  are the total wind turbine power, the free flow rate of the wind blowing into the wind turbine, the air density, and the swept area of the wind turbine can be calculated by  $A = \pi r^2$  (where  $r$  is the blade length of the wind turbine) and the pressure factor. The efficiency extracted by the wind turbine over the total amount present in the wind resource is called the power factor. Albert Betz calculated that a wind turbine could not convert more than 59.3% of the kinetic energy of the blowing wind into mechanical energy to rotate the rotor. This factor, known as the Betz Limit, is used for any wind turbine's theoretical maximum electrical power factor.

Figure 10 displays the final outcomes of the predicted power factor of the wind turbine's drive disc at different velocities. Each color pair represents the turbine's power factor under free flow and turbulent flow conditions when positioned on top of the building. The results reveal a significant increase in the turbine's power factor at wind speeds of 4 and 5 m/s. While a similar trend can be observed for other wind velocities, the power factor does not experience substantial growth as the wind speed further increases. Placing the wind turbine on top of a pitched roof building exposes it to higher wind velocities, leading to a notable increase in vortices surrounding the turbine blade and Karman vortices downstream. These vortices effectively reduce the kinetic energy in the wind flow, resulting in lower mechanical energy on the turbine shaft. Thus, it is advisable to install the wind turbine on top of a pitched roof building when the free flow velocity falls within the 4 to 5 m/s range.



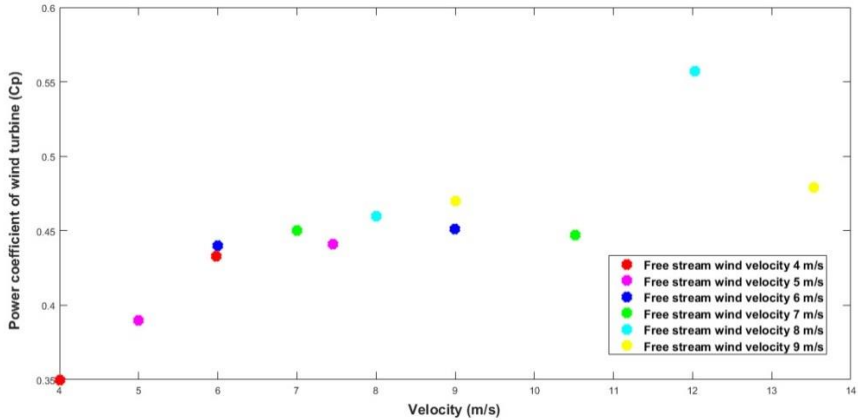


Fig.10. Compare the power factor of the wind turbine, at free-flow velocities of 4, 5, 6, 7, 8, and 9 m/s, with the power factor of the wind turbine

## 5 CONCLUSIONS

In conclusion, this study explored the performance of a small wind turbine positioned on top of a pitched roof building with a slope angle of  $27^\circ$ . The findings demonstrate a remarkable improvement in the turbine's power factor at wind speeds of 4 and 5 m/s, indicating the potential benefits of such installations in regions with moderate wind speeds. While a similar positive trend can be observed for other wind velocities, the power factor's growth does not exhibit significant increments as the wind speed increases further.

Moreover, the adoption of the actuator disc method in investigating the motion of wind turbine blades has provided valuable insights into the aerodynamics of the system. This research offers important reference data for the installation and efficient utilization of small wind turbines on high-rise buildings featuring inclined roofs. The findings have significant implications for promoting sustainable and clean energy solutions in regions where conventional wind turbines might not be as efficient, highlighting the potential of small wind turbines in enhancing energy generation from low to moderate wind speeds.

## References

1. L. Sara, Walker. Building mounted wind turbines and their suitability for the urban scale-A review of methods of estimating urban wind resources, *Energy and Buildings* 43(2011), pp 1852-1862.
2. J. Oliveira Paulo, A. Younis.Bassam, On the prediction of turbulent flows around full-scale buildings, *Journal of Wind Engineering and Industrial Aerodynamics*. 86 (2000), pp 203-220.
3. Y. Ozmen, E. Baydar, J.P.A.J. van Beeck, Wind flow over the low-rise building models with gabled roofs having different pitch angles, *Building and Environment* (2016).

4. G. M. Richardson, D. Surry, Comparisons of wind-tunnel and full-scale surface pressure measurements on low-rise pitched roof buildings, *J Wind Eng Ind Aerodyn* (1991)
5. T. Stathopoulos, K. Wang, H. Wu, Wind pressure provisions for gable roofs of intermediate roof slope, *Wind Struct* (2001).
6. D. Micallef, T. Sant, C. Ferreira, The influence of a cubic building on a roof mounted wind turbine. *Journal of Physics*. 753 (2016) 022044.
7. H. J. Wagner, J. Mathur, "Introduction to wind energy systems basics, technology and operation". Springer ISBN: 978-3-642-32975-3.
8. Wilcox, C. David. *Turbulence Modeling for CFD*. Second edition. Anaheim: DCW Industries, 1998. pp. 174.
9. J. E. Bardina, P. G. Huang, T. J. Coakley, *Turbulence Modeling Validation, Testing, and Development*, NASA Technical Memorandum 110446.
10. D. Scott-Pomerantz Colleen. *The K-Epsilon model in the theory of turbulence*. Ph. D. thesis. University of Pittsburgh.(2004)
11. R. Mikkelsen, *Actuator disk methods applied to wind turbines*. Ph. D. thesis. Technical University of Denmark.

**Open Access** This chapter is licensed under the terms of the Creative Commons Attribution-NonCommercial 4.0 International License (<http://creativecommons.org/licenses/by-nc/4.0/>), which permits any noncommercial use, sharing, adaptation, distribution and reproduction in any medium or format, as long as you give appropriate credit to the original author(s) and the source, provide a link to the Creative Commons license and indicate if changes were made.

The images or other third party material in this chapter are included in the chapter's Creative Commons license, unless indicated otherwise in a credit line to the material. If material is not included in the chapter's Creative Commons license and your intended use is not permitted by statutory regulation or exceeds the permitted use, you will need to obtain permission directly from the copyright holder.

